Nonlinear spatio-temporal emission dynamics of broad area laser diodes

Ingo Fischer[1], Ortwin Hess[2], and Wolfgang Elsäßer[1]

[1] Darmstadt University of Technology, Institute of Applied Physics, Schloßgartenstr. 7, D-64289 Darmstadt, Germany
[2] DLR, Institute of Technichal Physics, Pfaffenwaldring 38-40, D–70569 Stuttgart, Germany

Abstract. We present the combination of microscopic model calculations and direct experimental evidence for ultrafast nonlinear spatio-temporal dynamics of a laser system. In particular, we have studied the nearfield dynamics of a broad area semiconductor laser on picosecond timescales. The mechanisms inducing the complex behavior can be identified as self-focusing, diffraction, and hole burning. We find the onset of dynamical filamentation within the turn-on dynamics of such a laser and demonstrate that this is a non–transient behavior.

1 Motivation

Spontaneous spatio-temporal pattern formation has found rising interest in the field of nonlinear optical systems within the last decade (L. A. Lugiato et al. (1988)), (Abraham, Firth (1990)) The motivation to study optical systems in this context is twofold. On the one hand it has turned out that many transverse optical systems exhibit complex spatio-temporal dynamics covering a great variety of phenomena, partly showing close analogies to hydrodynamical or chemical systems. The specific advantages of optical systems is that various different geometries with different number of spatial dimensions can be easily realized, with different nonlinearities, good parameter control, easy near– and farfield investigations and with unique optical specifics as light polarization properties. The dynamical time scales of optical system cover ~ 12 orders of magnitude and range from seconds for photorefractive media down to picoseconds for semiconductor lasers. On the other hand the aim in laser design to move towards higher intensities is connected to the stronger influence of optical nonlinearities and to the realization of cavities with large apertures. Due to that, spontaneous pattern formation is often found to disturb laser applications and the detailed study of these phenomena will help to extend the knowledge about general properties of optical systems that have been disregarded for a long time.

In this contribution we present an optical system that exhibits complex spatio-temporal dynamics with one transverse spatial dimension and on ultrafast timescales, the broad area laser diode and its nearfield emission properties. Broad area laser diodes are designed as semiconductor lasers with high output power and therefore have large technological relevance. However, the increase in output power which is achieved by enlarging the transverse width of the active area from $w \sim 1\mu m$ for a usual narrow stripe laser to typical sizes of $w \sim 50\,\mu m$ to $500\,\mu m$ results in poor beam quality and coherence properties. This is related to the formation of transverse structures in the nearfield of the laser and the breakdown of the diffraction limitation in the corresponding farfield directionA, C, R. Recent experiments in combination with model calculations have given evidence for underlying strikingly complex spatio-temporal dynamics in the optical field O, O.

2 Modelling

Our simulations are based on the space-dependent Maxwell-Bloch equations for semiconductor lasers O which consist of a system of microscopic material equations selfconsistently coupled to the system of partial differential equations for the counterpropagating complex optical fields $E^+(x,z,t)$ and $E^-(x,z,t)$, the polarizations $P^+(x,z,t)$ and $P^-(x,z,t)$ as well as for the macroscopic charge carrier density $N(x,z,t)$

$$\pm\frac{\partial}{\partial z}E^\pm + \frac{n_l}{c}\frac{\partial}{\partial t}E^\pm = \frac{i}{2}\frac{1}{k_z}\frac{\partial^2}{\partial x^2}E^\pm - \left(\frac{\alpha}{2} + i\eta\right)E^\pm + \frac{i}{2}\frac{\Gamma}{n_l^2\epsilon_0 L}P^\pm \quad (1)$$

$$\frac{\partial}{\partial t}N = D_f\left(\frac{\partial^2}{\partial x^2} + \frac{\partial^2}{\partial z^2}\right)N + \Lambda - \gamma_{nr}N - W + G, \quad (2)$$

with the macroscopic generation rate

$$G = -\chi''\frac{\varepsilon_0}{2\hbar}\left(| E^+ |^2 + | E^- |^2\right) + \left\{\frac{(-i)}{2\hbar}\left[E^+ {P^+}^* + E^- {P^-}^*\right] + \text{c.c.}\right\}. \quad (3)$$

The macroscopic polarization variables are at every spatial point self-consistently linked to the microscopic polarization functions by summation over all momentum states $P^\pm = \frac{2}{V}\sum_{\mathbf{k}} d_{cv}(k)\, p^\pm_{\mathbf{r}}(k)$, where $d_{cv}(k)$ is the optical dipole matrix element; isotropic Fermi-surfaces are assumed, i.e. only $k = | \mathbf{k} |$ is considered. The dynamics of the *microscopic* polarization functions $p^\pm_{\mathbf{r}}(k)$ along with those of the distributions of electrons $f^e_{\mathbf{r}}(k)$ and holes $f^h_{\mathbf{r}}(k)$, where the index $\mathbf{r} = (x,z)$ indicates their parametrical dependence on space, is governed by the microscopic system of material equations presented and discussed in O, O. In the macroscopic wave equations (1), passive wave-guiding properties are represented by $\eta = \eta(x)$ and the confinement factor $\Gamma = \Gamma(x)$ O. The (linear) refractive index of the semiconductor material is denoted by n_l, c is the speed of light, $L = 200\mu m$ the total (longitudinal) length of the laser cavity and ϵ_0 the permittivity of free space. The wave number in (longitudinal) propagation direction is given by $k_z = n_l k_0$, with k_0 being the unperturbed wave number in the vacuum. In (1) and in the generation rate (3), the linear part of the polarization is conveniently included in the linear absorption term α of the semiconductor and in the imaginary part of the susceptibility O, $\chi'' = \alpha n_l^2/2\pi\lambda$, respectively, with λ being the wavelength of laser. Diffusion of charge carriers is represented in (2) via the diffusion coefficient D_f, where the influence of spatial variations of N on D_f is disregarded. The rates of nonradiative and spontaneous recombination are given by γ_{nr} and W, respectively O. The transversely dependent injection of charge carriers along the contact stripe is represented by the pumping term $\Lambda(x) = j(x)\eta_i/ed$, where the current density $j(x)$ is uniform along z and transversely only different from zero from $x_0 - w/2 \leq x \leq x_0 + w/2$, x_0, being the center of the laser stripe, $w = 100\mu m$ its width and $\eta_i = 0.8$ the fraction of carriers which actually reaches the active region; e is the electron charge and $d = 0.15\mu m$ the (vertical) thickness of the layer. The *longitudinal boundary conditions* are given by $E^+(x, z=0, t) = -\sqrt{R_1}\, E^-(x, z=0, t)$ and $E^-(x, z=L, t) = -\sqrt{R_2}\, E^+(x, z=L, t)$. They represent reflection of the optical fields at the facet mirrors at $z = 0$ and $z = L$ of the laser structure. The *transverse boundary conditions* $\partial E^\pm/\partial x = -\alpha_w E^\pm$ and $\partial N/\partial x = -\tilde{v}_{sr} N$ at $x = +w/2$ as well as $\partial E^\pm/\partial x = +\alpha_w E^\pm$ and $\partial N/\partial x = +\tilde{v}_{sr} N$ at $x = -w/2$ account for the strong absorption (constant α_w) of the optical fields outside the pumping stripe and surface recombination effects of the charge carriers.

3 Experimental Methods

Before directly comparing our numerical results with corresponding experimental ones we present a short outline of our experiments. The measurements of the turn-on dynamics in the near–field of the broad area laser (BAL) have been performed using a GaAs/GaAlAs laser (SDL-2430-C) emitting at $\lambda = 814nm$. Its active region incorporating a quantum well active layer structure has a transverse width of $w = 100\mu m$. The threshold current of the laser is $I_{th} = 290\, mA$.

The measurement of the spatio–temporal near–field dynamics requires the detection of single events with ps–time resolution and μm spatial resolution. For this reason we make use of a single–shot streak camera technique. The experimental setup is schematically depicted in Figure 1. A magnified image of the near-field of the light intensity emitted at the output facet is obtained using a microscope objective which projects the output facet of the laser onto the input slit of a Hamamatsu streak camera C1587 with a single sweep unit M1952. This allows to measure single-shot spatio-temporal traces with a temporal resolution down to $\sim 10ps$. The main pulse generator serves as current source for the broad area laser and as trigger source for the streak camera and a second trigger generator. The broad area laser is driven with rectangular pulses of $25ns$ length with a rise time of about $3ns$. The repetition rate of the pulses is 100 Hz which ensures that junction heating can be minimized which otherwise would additionally contribute to thermal lensing effects. The amplitude of the pulses corresponds to an injection current of

~ 2 times the threshold current. The streak camera is triggered by one single, arbitrarily chosen pulse delayed with respect to the current pulse, allowing to choose the temporal position of the spatio-temporal near-field traces. The traces which are visualized on the phosphor screen of the streak tube are read out by a cooled high–sensitivity CCD-camera which is linked to a computer via a frame grabbber card where the traces can be stored.

For these driving conditions the laser emits several transverse (and longitudial) modes corresponding to a spectral width of less than 2 nm which is obtained from time-integrated measurements by an optical spectrum analyzer. The time-integrated near-field shows a nearly periodic spatial modulation of the intensity, consisting of different transverse modes, which is a well known behavior called multi-filamentation, fundamental solitons or higher nonlinear modes. D, C, R, D, G. Under these operation conditions complex spatio-temporal behavior can be observed, as we will demonstrate in the following.

4 Experiments and Modelling Results

In the following we shall present and discuss the spatio-temporal intensity traces, extracted from the numerical modelling and directly compare them to those obtained in the measurements. In the first part we concentrate on the first $4.8ns$ after applying the current pulse to the laser. Fig.2 a) depicts a numerically obtained nearfield trace, Fig. 2 b) an experimental streak trace for $I = ...$ The x–axis represents the position on the output facet of the BAL. The emitted intensity is linearly coded via greyscales such that light shading corresponds to high intensities and dark shading to low intensities. The temporal evolution is depicted in the y–direction. The time window depicted here has a length of $4.8ns$. The modelled trace in Fig. 2 a) exhibits a spatially nearly homogeneous relaxation oscillation as response of the semiconductor laser to the current pulse. Starting already with the second relaxation oscillation the pulse breaks up into seperate spots ending up in an irregular spatio-temporal emission dynamics. The experimental trace in Fig. 2 b) also shows a spatially nearly homogeneous relaxation oscillation in the first 1.5 ns. The emission intensity at the right edge of the active area for $80\mu m \leq x \leq 100\mu m$is a little bit lower which, however, has evolved after some ns to be the same as at other lateral positions. In correspondence with the modelling the intensity profile breaks up already after this first relaxation oscillation into seperate spots of high emitted intensity. The time of the second relaxation oscillation peak varies for different lateral positions. After the first relaxation oscillation peak the emission intensity is modulated in the lateral direction showing 7 maxima. This modulation is present for the following temporal evolution of the intensity. This nearly static modulation is well-known as multi–filamentation or higher nonlinear modes. We want to concentrate here on the dynamical changes within the lateral beam profile.

5 Discussion

6 Conclusion

References

L. A. Lugiato, F. Prati, L. M. Narducci, P. Ru, J. R. Tredicce, D. K. Bandy (1988) Phys. Rev. **A 53**, 3847

N. B. Abraham and W. Firth, J. Opt. Soc. Am. B. **7**, 951 (1990).

L. A. Lugiato, Chaos, Solitions & Fractals, **4**, 1251 (1994).

. G. Harrison, J. S. Uppal (editors), "Nonlinear Dynamics and Spatial Complexity in Optical Systems", SUSSP Proceedings **41** (1992).

. Hess and T. Kuhn, Prog. Quant. Electr., **20**, 85 (1996).

. Hess, Chaos, Solitons & Fractals **4**, 1597 (1994).

. Hess, S. W. Koch, and J. V. Moloney, IEEE J. Quant. Electr., **QE-31**, 35 (1995).

. Larsson, J. Salzman, M. Mittelstein, and A. Yariv J. Appl. Phys. **60**, 66 (1986).

. J. Chang-Hasnain, E. Kapon, E. Colas, IEEE J. Quant. Electr., **QE-26**, 1713 (1990).

. J. Lang, A. G. Larsson, J. G. Cody, IEEE J. Quant. Electr., **QE-27**, 312 (1991).

. W. Mc Laughlin, J. V. Moloney, A. C. Newell, Phys. Rev. Lett., **51**, 75 (1983).

. Khitrova, H. M. Gibbs, Y. Kawamura, H. Iwamura, T.Ikegami Phys. Rev. Lett., **70**, 920 (1993).

. Fischer, O. Hess, W. Elsäßer, unpublished

. K. DeFreez, D. J. Bossert, N. Yu, K. Hartnett, R. A. Elliott, Appl. Phys. Lett., **53**, 2380 (1988).

. Mehuys, R. J. Lang, M. Mittelstein, J. Salzman, A. Yariv, IEEE J. Quant. Electr., **QE-23**, 1909 (1987).

. H. Paxton, G. C. Dente J. Appl. Phys., **70**, 2921 (1991).

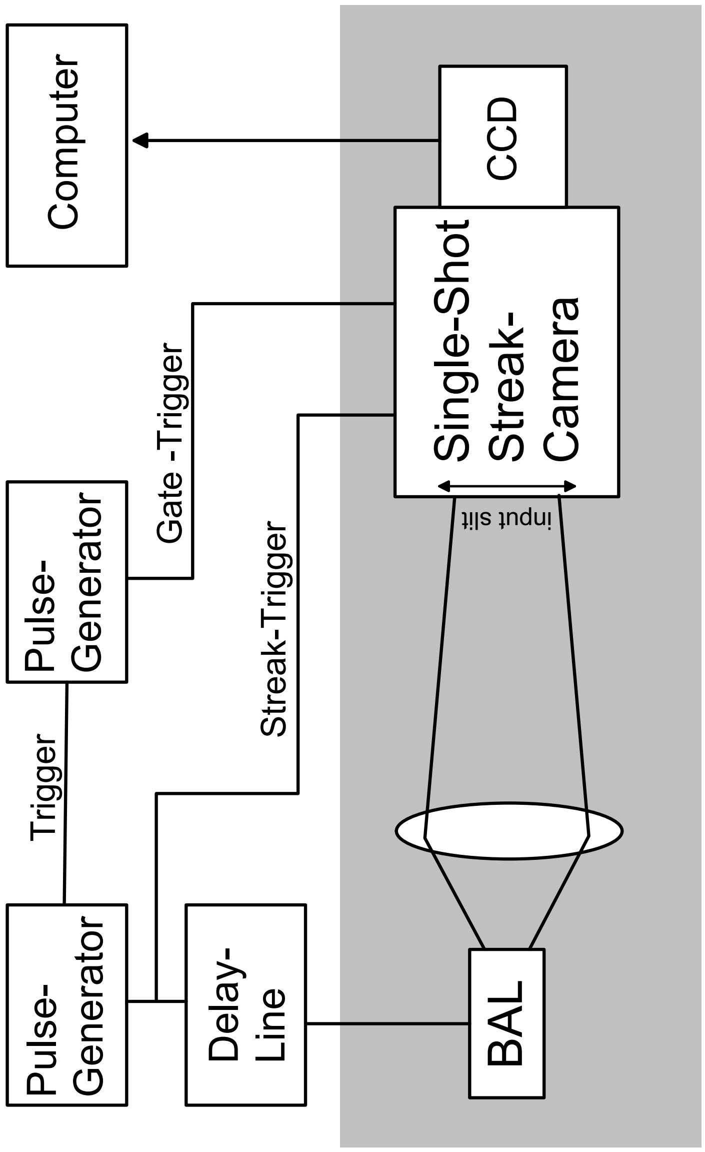

Fig. 1. Experimental setup for spatio-temporal near-field measurements of a broad area semiconductor laser